Unusual catalytic hydrogenation caused by photoinduced solid frustrated Lewis pairs

Zhen Wan [a,c], Chengjun Wang [c], Chun Yang [a,b], Dongge Ma [d], Hongwei Ji [a,b], Chuncheng Chen [a,b], Wanhong Ma [a,b,*], Jincai Zhao [a,b]

[a] *Key Laboratory of Photochemistry, CAS Research/Education Center for Excellence in Molecular Sciences, Institute of Chemistry, Chinese Academy of Sciences, Beijing 100190, PR China*
[b] *University of Chinese Academy of Sciences, Beijing 100049, PR China*
[c] *Key Laboratory of Catalysis and Materials Science of the State Ethnic Affairs Commission and Ministry of Education, College of Resources and Environmental Science, South-Central Minzu University, Wuhan 430074, PR China*
[d] *College of Chemistry and Materials Engineering, Beijing Technology and Business University, Beijing 100048, PR China*

ARTICLE INFO

ABSTRACT

Most homogeneously FLP-catalyzed hydrogenation reactions that follow cleavage of H_2 occur via protonation of substrates followed by hydride transfer. This order of activated H-transfer unavoidably limits the application scope of currently FLP-catalyzed hydrogenation to nucleophilic substrates. Herein, we report an unusual inverse H-transfer order in which photoinduced solid In_2O_3-FLPs catalyze the hydrogenated dehalogenation of aryl halides with H_2. After the generation of active FLPs of In-OH$^+$ and In-[O_v]H$^-$ via H_2 splitting on In_2O_3 surface upon irradiation, a series of aryl halides were readily activated and initiated at the In-[O_v]H$^-$ sites and then dehalogenated with high yields. By combining this work with detailed studies on H/D kinetic isotope effects and activation energies of hydrogenated dehalogenation, we demonstrate that initial hydride transfer mediated by photoinduced solid FLPs is more effective than common proton transfer to initiate hydrogenation of these substrates.

1. Introduction

Catalytic activation of the H-H bond in molecular hydrogen for hydrogenation reactions has been widely studied and applied in the areas of petrochemistry, fine chemical syntheses and solar energy conversion and storage [1–6]. Recently, frustrated Lewis pairs (FLPs), in which the formation of classic Lewis acid-base adducts via dative bonds between Lewis acid and base sites is sterically hindered, have become a promising kind of catalyst for the hydrogenation of various unsaturated substrates [7–10]. In these catalysts, the independent H$^-$ and H$^+$ moieties formed upon dissociation of H_2 coexist on one catalyst molecular framework, such as a phosphine-borane (P-B) structure, and bond with Lewis acidic and basic sites as zwitterionic phosphonium-borohydride, respectively. Since Stephan's group first achieved aromatic hydrogenation of anilines to afford cyclohexylamine derivatives [11], the metal-free homogeneous hydrogenation catalyzed by such FLPs and the corresponding dynamic characteristics for a broad range of substrates with polarized double

bonds or unpolarized alkenes and alkynes have been widely investigated [12–16]. The hydrogenation of substrates with polarized double bonds almost starts with proton transfer into the unsaturated bonds of the substrates, followed by attack by hydride H$^-$ ions, regardless of whether the target substrates have electron-deficient or electron-rich substituents [17]. That is, the FLP catalysts first transfer a proton to the substrate, forming a carbocation intermediate, and then spontaneously undergo hydride transfer to generate the hydrogenated end-products (Scheme 1 a). This occurs because the [Ar₃BH]$^-$ moiety is less active than the [R₂PH]$^+$ moiety in the ubiquitous P-B FLP catalyst, in which the borane moiety is a very strongly electron-withdrawing fluoroaryl substituent commonly used as a Lewis acid site. Thus, the [Ar₃BH]$^-$ moiety of a P-B-based FLP is not a sufficiently strong hydride donor to induce the hydrogenation of most substrates except for a limited number of examples, such as strongly electron-deficient α,β-unsaturated compounds [18,19]. This characteristic of P-B-based FLPs significantly limits the substrate scope of those with unfavorable protonation, such as arenes

---
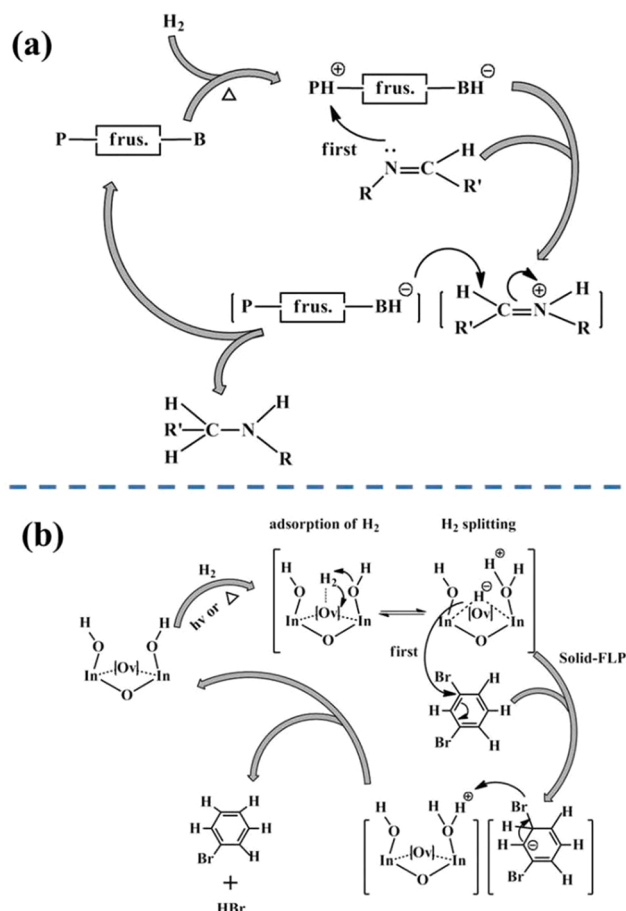
Scheme 1. Schematic diagrams. (a) Hydrogenation of imines by a traditional homogeneous P-B FLP catalyst. (b) Hydrogenation dehalogenation by photo-induced solid FLPs in this work, in which inverted hydride ion transfer from In-[O_v]H- occurs first.

[17].

Recently, heterogeneous FLP catalysis based on metal oxides has attracted considerable interest in the field of catalytic hydrogenation because it involves H_2 and other environmentally friendly hydrogen donors, such as alcohols [20]. Analogous to the P-B-based homogeneous FLPs in the activation of H-H bonds to form H^+ and H^- moieties, O^{2-} and M^{n+} sites on the surface of solid (MO_x) serve as Lewis basic (LB) and Lewis acidic (LA) sites, respectively [20,21]. Several metal oxides have been developed to dissociate H-H bonds as solid FLPs. For example, hydrogenation reactions of some small molecules, such as CO_2, alkynes and aldehydes, have been successfully achieved by solid FLP catalysts in recent years [22–24]. In particular, In_2O_3, as a potential solid-FLP, was applied to realize diverse hydrogenation reactions [25–27]. Ozin et al. reported that rh-$In_2O_{3-x}(OH)_y$ can activate H_2 via surface FLPs even at room temperature [20]. Although the solid FLP role of transition metal oxides such as In_2O_3 in the catalytic dissociation of H-H bonds has been identified [28], whether the transfer order and activity of protons/hydrides are similar to those of homogeneous P-B PLPs is not completely clear. In principle, since the electron-withdrawing effect of transition metal oxide FLPs can be controlled to less than that of the [Ar_3BH]- moiety of P-B-based FLPs, it is possible for the [M^{n+}-H]- group to exhibit more activity than [Ar_3BH]- to react with substrates that are not readily activated by either the [R_2PH]+ moiety or the [Ar_3BH]- moiety of P-B FLPs. Furthermore, since the empty orbital of the transition metal exhibits different acceptor features than the p-orbital of the Ar_3B molecule, the formed hydride complex can be photoexcited to a very high-energy state, and the resulting hydride ions can readily

activate inert substrates that are unable to first undergo protonation. This protocol is apparently useful for overcoming the defects of homogeneous P-B FLPs in hydrogenation reactions that are unfavorable for conventionally nucleophilic protonation, such as the hydrogenated dehalogenation of aryl halides.

Since the major toxicities of aromatic halides attribute to the halogenated groups that have led to serious threats to the ecological environment, the specialized degradation of such compounds, even only hydrogenated dehalogenation into their arene parents, is still an important approach in environmental fields [29,30]. The common alternatives for the hydrogenated elimination of aromatic halides are the anaerobic biological treatment, nano zero-valent iron reduction, transition/noble metals-based catalytic reduction and photocatalytic reduction and so on [31]. Among them, the anaerobic biological treatment could effectively degrade the aromatic halides with multiple halogen substitution albeit it usually requires a long reaction times and the limited reaction conditions such as room temperature and suitable pH value as well as ineffective to these low halogenated compounds [32–34]. Nano zero-valent iron (NZVI) reduction is widely studied in the area of dehalogenation degradation through stoichiometric oxidation of NZVI into Fe(II) under anaerobic conditions [35–37]. The transition metals-based catalytic reactions can also be used for the dehalogenation of aromatic halides. For instance, Lei et al. prepared Cu/TiO_2 nanocomposites for the debromination of 2,2′,4,4′-Tetrabromodiphenyl ether (BDE47), in which the debromination efficiency reached 87.7% in 3 s with the addition of hydrazine hydrate ($N_2H_4 \cdot H_2O$) [38]. They further indicated that the Pd/TiO_2 as catalysts yielded effective debromination of BDE47 in isopropanol solution containing NaOH at 40 °C within 60 min [39]. Alternatively, photocatalytic reductions, generally involves the use of alcohols as hydrogen sources to succeed in reductive dehalogenation of diverse organic halides, in which the aldehydes formed via alcohol oxidation are detrimental by-products [40,41]. Therefore, considering the high efficiency of solid-FLPs in other hydrogenation reactions [42–44] and the characteristics of no secondary pollution in H_2 dissociation of itself, the exploration of H_2-based hydrogenation of aryl-compounds by solid-FLPs is needed today. In comparison to other transition metal oxides, cubic In_2O_3 (c-In_2O_3) is recently revealed as a potential solid FLP catalyst for the hydrogenated dehalogenation of aromatic halides [44]. In_2O_3, especially rhombohedral polymorph, rh-$In_2O_{3-x}(OH)_y$, is readily to form the typical non-stoichiometric metal oxide containing abundant oxygen defects that is easy to form separately Lewis acidic and basic sites on the surface [21,45]. Different from unmanageable non-stoichiometric rh-$In_2O_{3-x}(OH)_y$, the common c-In_2O_3 as FLP catalysts are more worth looking forward to. This is due to their easy fabrication and high-repeatable stability. Moreover, the numbers of [LB-H]- sites on c-In_2O_3 surface arisen from H_2 decomposition maybe significantly increase upon the UV irradiation through its special stabilization and charge transfer characteristic of In-H bond of c-In_2O_3 [46].

In this work, through detailed H/D kinetic isotopic effect investigations and spectroscopic characterization, we report that upon light irradiation, c-In_2O_3 as a solid-FLP can facilitate hydride ion transfer prior to the protonation of some inert aryl halides when H_2 is used as the hydrogen source. By comparison with studies in which ethanol was used as a hydrogen source and c-In_2O_3 served as a normal proton-coupled electron transfer (PCET) photocatalyst, we confirmed that c-In_2O_3 exhibits a solid-FLP nature only when H_2 is used as a hydrogen donor. The resulting hydride can be stabilized at the In sites on the c-In_2O_3 surface, as observed by solid-MAS-^{1}H NMR (Scheme 1b). Hydrogenated dehalogenation of a series of aryl halides mediated by c-In_2O_3 photocatalysts in the presence of H_2 at 140 °C showed much less activation energy and higher yields than similar reactions with alcohol as the hydrogen source under identical conditions. Our results highlight for the first time the feasibility of hydride ion transfer prior to protonation to achieve the smooth hydrogenation of aromatic halides that are inert toward homogenous FLP-catalyzed hydrogenation reactions.
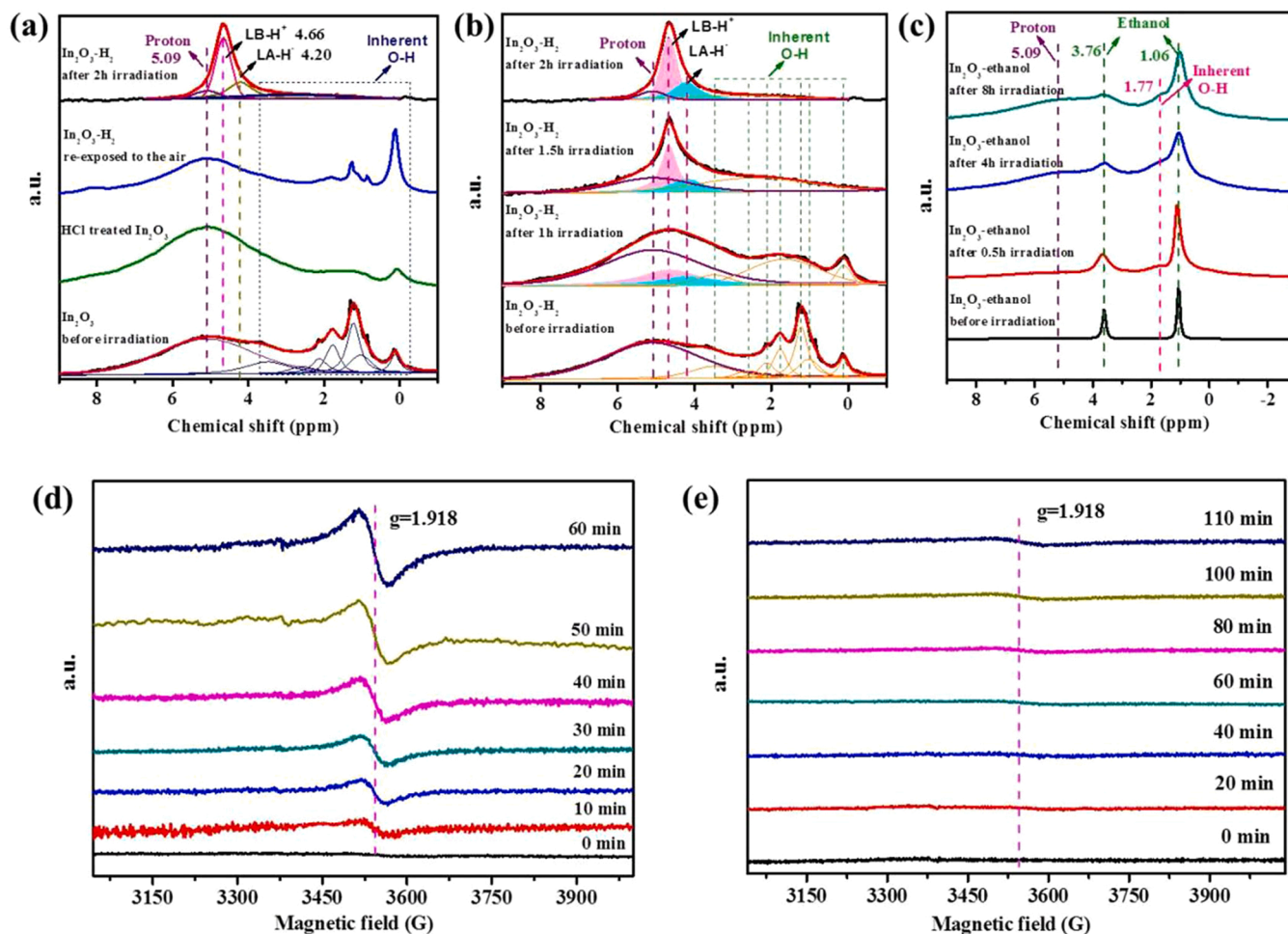
Fig. 1. MAS-^{1}H NMR and ESR spectra of c-In$_2$O$_3$ under different irradiation conditions. (a) MAS-^{1}H NMR spectra of c-In$_2$O$_3$ samples irradiated in the presence of H$_2$ for 2 h, air-exposed c-In$_2$O$_3$ samples after irradiation in H$_2$ for 2 h, c-In$_2$O$_3$ samples treated with hydrochloric acid solution (0.1 M) for 1 h and c-In$_2$O$_3$ samples before irradiation. (b-c) Solid-state ^{1}H NMR spectra of c-In$_2$O$_3$ samples after irradiation in the presence of H$_2$ (b) and ethanol (c) for different times. (d-e) Low-temperature (90 K) ESR spectra of c-In$_2$O$_3$ samples after irradiation in the presence of ethanol (d) and H$_2$ (e) for different times.

2. Experimental section

2.1. Material synthesis

The synthesis of c-In$_2$O$_3$ nanoparticles has been described in detail elsewhere [25]. Typically, 3.6 g of indium(III) chloride was dissolved in a mixture of ethanol (54 mL) and deionized water (18 mL). Then, another mixed solution with 54 mL of ethanol and 18 mL of ammonium hydroxide (25 wt%) was rapidly added to form a white precipitate. The resulting suspension was immediately moved to a preheated oil bath at 80 °C. After stirring for 15 min, the suspension was removed and cooled to room temperature. The precipitate was centrifuged and washed with deionized water 5 times and then dried in a freeze drying oven overnight. The collected precursor was calcined for 3 h in air at 250 °C.

2.2. Characterizations

Powder XRD was performed on a Regaku D/Max-2500 diffractometer using a Cu Kα radiation source. X-ray photoelectron spectroscopy (XPS) analysis was carried out by using a Thermo ESCA-Lab250Xi spectrometer with monochromatic Al Ka radiation. All binding energies were referenced to the C 1 s peak at 284.63 eV. TEM studies were conducted on a Tecnai G2 F20 S-TWIN electron microscope operated at an accelerating voltage of 200 kV. UV–vis absorption spectra were obtained by a Hitachi U-3010 spectrophotometer using BaSO$_4$ as the reflectance sample.

2.3. MAS-1H NMR measurements

MAS-^{1}H NMR analyses were carried out in a 400 MHz Bruker nuclear magnetic resonance spectrometer. The as-prepared samples were transferred into a zirconia rotor (4 mm in diameter) at room temperature in an Ar glove box, and then the rotors were sealed for measurements immediately. For the acid-treated samples, 0.2 g of the catalysts was stirred in HCl aqueous solution (0.1 mol/L) for 2 h and then dried at room temperature before the measurements. Furthermore, for the re-exposed c-In$_2$O$_3$ samples, 0.2 g of the catalysts irradiated in H$_2$ were kept in air for 24 h at room temperature before the measurements. The chemical shifts were calibrated by adamantane at 1.91 ppm.

2.4. Electron spin resonance spectrum measurements

The signals for e$_{cb}^-$ of the c-In$_2$O$_3$ samples after light irradiation in the presence of H$_2$ or ethanol for different reaction times were explored by electron spin resonance (ESR) spectroscopy. The samples were sealed in quartz tubes in an Ar atmosphere. The instrument was a Brucker ESP 300 E spectrometer with a sweep width of 1000 Gs, and the low temperature (90 K) was maintained by liquid nitrogen.

2.5. Photocatalytic dehalogenation reactions

The H_2 used in the experiments was produced by a hydrogen generator purchased from the Beijing BCHP Analytical Technology Institute. The light source was a 300 W Xenon lamp (CEL-HXF300, Beijing) with a 330 nm cutoff filter. Decane was used as the solvent in all experiments. The reaction was carried out in a Pyrex vessel with a volume of 160 mL, which was sealed with a rubber septum. In a typical reaction, 0.2 g of the as-prepared catalysts was added to 15 mL of substrate solution (2.5 mmol/L). The suspension was deaerated for 1 h with purging H_2 (120 mL/min), magnetically stirred for 30 min to reach adsorption-desorption equilibrium in the dark and then kept at the desired reaction temperature during irradiation. In contrast, the as-prepared catalyst was also irradiated with ethanol. The reaction was performed under Ar, and 0.8 mL of ethanol was added along with the substrate solution. The products were analyzed by gas chromatography with a solution of 1,2-dichlorobenzene or fluorobenzene as the internal standard. Ion chromatography (IC) analyses were also used to detect the concentration of produced bromide ions. A 15 mM KOH solution was chosen as the eluent for the measurements. The current was 50 mA, and the flow rate was 0.7 mL/min. Kinetic isotope effect values were defined as the ratio of the conversion rate for substrates in H_2 and D_2 or in ethanol and ethanol-d_6.

3. Results and discussion

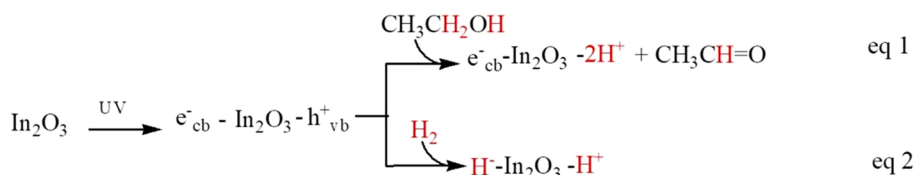### 3.1. Confirming the photoinduced FLP structure on the c-In_2O_3 surface

In the activation of H_2 catalyzed by solid FLP catalysts, the first step is decomposition of the H-H bond in H_2 into available [LA-H]$^-$ and [LB-H]$^+$ forms on the surface of oxide nanoparticles [47]. Despite the results of theoretical calculations and simulations indicate that c-In_2O_3 can decompose H_2 into separated In-H$^-$ and O-H$^+$ sites on the surface, direct experimental evidence for the formation of hydride moieties on the solid surface is still scarce. Therefore, we first investigated whether and where the [LA-H]$^-$ and [LB-H]$^+$ ion pairs can exist on the surface of common c-In_2O_3 nanoparticles upon photoirradiation. To this end, we synthesized sheet-like c-In_2O_3 nanoparticles with classic cubic structures [45] by a hydrothermal/calcination method, and the general characteristics are determined, as shown in Fig. S1. Before the c-In_2O_3 samples were used to photocatalytically hydrogenate aryl halide substrates by H_2, we took advantage of different characteristic methods to trace [LA-H]$^-$ and [LB-H]$^+$ ion pairs formed by H_2 decomposition on the surface of c-In_2O_3 nanoparticles upon irradiation (Fig. 1). In addition, ethanol, which is a well-known hole scavenger that can generate protons, aldehydes and trapped electrons in the conduction band, was used as another hydrogen source with the same c-In_2O_3 samples as a control. [LA-H]$^-$ and [LB-H]$^+$ ion pairs formed by decomposing H_2 on the surface of c-In_2O_3 nanoparticles upon photoexcitation were directly studied by solid-state ^1H NMR spectra with H_2 and ethanol, as shown in Fig. 1a-c. In Fig. 1a, several peaks can be observed in the range of 0.12–5.09 ppm for the c-In_2O_3 sample in the presence of H_2 before irradiation. The broad peak at 5.09 ppm was identified as the hydrogen signal of residual protons from adsorbed water, while the seven individual peaks at 0.12, 1.03, 1.22, 1.77, 2.12, 2.58 and 3.5 ppm were attributed to the inherent hydrogen in the c-In_2O_3 sample, as previously reported [48] and further confirmed by a control experiment in which the c-In_2O_3 sample was preprocessed by an HCl solution to increase the proton content in the sample (Fig. 1a, green). In that curve, the intensity of the peak at 5.09 ppm was evidently increased relative to the intensity of the inherent hydrogen peak (0.12–3.5 ppm), as the inherent hydrogen is difficult to protonate. In addition, a new peak at 4.66 ppm was formed after irradiation of the sample for 2 h (Fig. 1a, black), and this peak could be divided into three individual signals (5.09, 4.66 and 4.20 ppm). In Fig. 1b, as with the spectrum of the H_2/c-In_2O_3 sample irradiated by Xe light, peaks at 4.66 and 4.20 ppm clearly appeared and increased

significantly with increasing irradiation time, until the peaks gradually overlapped with the 5.09 ppm signals. As H_2 was completely consumed, the peaks at 4.66 and 4.20 ppm were eventually covered by other signals. Compared with the original proton peak at 5.09 ppm, the peak at 4.66 ppm was tentatively attributed to the [LB-H]$^+$ signal, while the peak at 4.20 ppm was identified as the [LA-H]$^-$ signal resulting from cleavage of the H-H bond. This conclusion was very well supported by re-exposing the c-In_2O_3 samples to air for 6 h, after which the peaks at 4.66 and 4.20 ppm disappeared while others, including the original proton peak at 5.09 ppm, remained unchanged (Fig. 1a, blue). The peak at 4.66 ppm attributed to [LB-H]$^+$ was consistent with the previous observation that the classic Lewis basic sites of c-In_2O_3 are hydroxide moieties proximal to oxygen defects [49]. To further confirm this solid-FLP [LA-H]$^-$ reality during photocatalytic H-H bond breaking, we used ethanol as a hole scavenger under identical conditions to determine whether [LA-H]$^-$ was generated. In Fig. 1c, before irradiation, the peaks at 3.76 and 1.06 ppm were ascribed to the hydrogen from the methylene hydroxyl and methyl groups of the ethanol loaded on the c-In_2O_3 sample, while the peak at 5.09 ppm attributed to the original protons of c-In_2O_3 was too weak to discern due to the absolutely dominant signals of ethanol. Upon irradiating the c-In_2O_3 sample treated with ethanol, the peaks at 1.06 and 3.76 ppm constantly decreased with irradiation time, and the peaks at 5.09 and 1.77 ppm attributed to the original protons of c-In_2O_3 reappeared. These results clearly demonstrated that ethanol on c-In_2O_3 was increasingly depleted with irradiation time and generated protons that increased the proportion of c-In_2O_3 surface protons. However, above all, the signals at 4.66 and 4.20 ppm, which were assigned to the [LB-H]$^+$ and [LA-H]$^-$ signals corresponding to the original protons, respectively, were never observed in the ethanol-treated samples (Fig. 1c). This indicated that photocatalysis of c-In_2O_3 in ethanol as a hole scavenger normally generates aldehyde, releases protons and traps electrons within the conduction band of c-In_2O_3, similar to most metal oxide photocatalysts, such as TiO_2 and ZnO [40,50,51], although the signal of the aldehyde product was not clearly distinguished (in Fig. 1c), likely due to the influence of the relatively strong ethanol signal. Moreover, we provide important ESR evidence to differentiate the effect of H_2 relative to that of ethanol as a hole scavenger that leads to solid-FLP [LA-H]$^+$/[LB-H]$^-$ or trapped H$^+$-In_2O_3/e$^-_{cb}$.

ESR measurements were performed to compare the trapped electrons in c-In_2O_3 samples with either ethanol or H_2 as a photocatalytic hydrogen source. For the samples in the ethanol case, a strong signal at g = 1.918 was observed that increased obviously with increasing irradiation time (Fig. 1d). This is the typical signal of photoinduced and then trapped electrons on metal oxide semiconductors and is in good agreement with most reported observations when ethanol is used as a hole scavenger under anaerobic conditions [51,52]. That is, the signal (g = 1.918) is distinct as the electrons trapped and delocalized on the conduction band of c-In_2O_3 [51,52]. In contrast, for the samples irradiated in the H_2 case (Fig. 1e), the same signal was not observed. In fact, the total concentration of accumulated electrons available from c-In_2O_3 under H_2 conditions is much higher than that in the ethanol case upon titration via the Fe(III)−1,10-phenanthroline spectrophotometric method (Fig. S2). Moreover, as shown in Fig. S3, no ESR signals were observed for the samples before irradiation or after irradiated in the absence of ethanol and H_2 under Ar conditions. Both the ESR and electron titration results strongly indicated the formation of active paired electron H$^-$ species on c-In_2O_3 in the H_2 case that could not be observed by ESR but could be titrated by two equivalents of Fe(III). Thus, concluded from the MAS ^1H NMR and ESR results that in the ethanol case, the photogenerated holes (h$^+_{vb}$) participate in H$^+$ formation from the oxidizing hydrogen of organic hydrocarbons, while photogenerated electrons remain in the conduction band as delocalized or localized electrons (e$^-_{cb}$). This is quite consistent with most well-known photocatalytic cases (eq 1). However, in the H_2 case, which is considerably different from the ethanol case, photoexcited c-In_2O_3 formed holes and electrons that were incorporated into the cleaved H-H bond

during paired-electron transfer, resulting in a metastable $[LB\text{-}H]^+/[LA\text{-}H]^-$ FLP (eq 2). That is, there were no remaining single electrons or holes in the conduction band or valence band of c-In_2O_3, as they were converted into hydride ions and proton species, respectively, in the form of $[LB\text{-}H]^+/[LA\text{-}H]^-$.

species such as protons to form hydroxides (1.195 e⁻), which corresponds to the changes in the XPS results (Fig. S5). Hence, it is reasonable to infer that H_2 was first adsorbed on the oxygen vacancy and then heterolytically split into proton and hydride ions upon irradiation and at the proper reaction temperature. In the former case, the hydrogen was

$$In_2O_3 \xrightarrow{UV} e^-_{cb} \text{-} In_2O_3 \text{-} h^+_{vb}$$

$$\xrightarrow{CH_3CH_2OH} e^-_{cb}\text{-}In_2O_3 \text{ -}2H^+ + CH_3CH=O \qquad \text{eq 1}$$

$$\xrightarrow{H_2} H^-\text{-}In_2O_3 \text{ -}H^+ \qquad \text{eq 2}$$

3.2. Understanding the photocatalytic dissociation pathway of H_2 by c-In_2O_3

Previous studies of the Lewis basic sites of c-In_2O_3 indicated that the hydroxide groups in the inherent structure of $In_2O_{3-x}(OH)_y$ became more basic and hence more active upon irradiation [45,49]. However, this assumption was not consistent with our MAS-^{1}H NMR results, in which no peak attributed to the $[LB\text{-}H]^+$ moiety was observed for the c-In_2O_3 samples before irradiation (Fig. 1a). Thus, we argue that the LB site of c-In_2O_3 must be formed in situ at the beginning of the hydrogenation reactions. Similar to the results for other metal oxides [53–58], our XPS determination of the O1s spectrum confirmed the presence of chemisorbed oxygen on the c-In_2O_3 surface, which displayed a higher binding energy than lattice oxygen (Fig. S1). DFT analyses (Fig. S4a-b) revealed that these chemisorbed oxygen were located at the sites of oxygen defects and possessed lower negative charges (0.700 e⁻) than lattice oxygen (1.006 e⁻). During irradiation under a H_2 atmosphere, the number of chemisorbed oxygen decreased, and the binding energy for the whole spectrum shifted to a lower position, in contrast to the samples irradiated in the presence of ethanol, demonstrating that these chemisorbed oxygen served as active sites in the reaction (Fig. S5). In addition, we calculated the adsorption energy of hydrogen on chemisorbed and lattice oxygen and found that the adsorption energy of hydrogen on chemisorbed oxygen (−3.07 eV) was much lower than that of hydrogen on lattice oxygen (−1.01 eV), which means that hydrogen species prefer to bond with chemisorbed oxygen (Fig. S4c-d). Moreover, according to Bader charge analysis, the chemisorbed oxygen showed an evident increase in their negative charges after bonding with hydrogen

transferred to the positions of surface chemisorbed oxygen to form hydroxide, serving as the Lewis basic sites; in the latter case, the hydrogen was transferred to the In sites adjacent to the oxygen vacancy (Scheme 2a), consistent with the DFT calculations (Fig. S4e). Upon irradiation, independent H^+ and H^- ions were exactly formed on the surface of c-In_2O_3, which were proposed to be bonded with hydroxide groups and indium atoms proximal to oxygen defects. Notably, in the ethanol case (Scheme 2b), H^+/e^-_{cb} was not converted into $[LA\text{-}H]^-$, indicating that the photoexcitation in the H_2 case (i.e., in ESR, there was no common e^-_{cb} feature) likely differs from that in the ethanol case. In the presence of H_2, the excitation of c-In_2O_3 is never the traditional photocatalytic basis for the generation of true h^+_{vb} and e^-_{cb} to react with different objects; instead, concerted reaction occurs with the same substrate, H-H molecules inject h^+_{vb} to generate H^+ and inject e^-_{cb} to generate H^-. This is probably because surface hydroxides and the sites of oxygen defects on c-In_2O_3 readily become the center of both e^-_{cb} and h^+_{vb} trapping, while there are no available hole scavengers, such as alcohol [59]. Namely, once no C-H, C-O or C-OH bonds, such as those in the ethanol molecule, are available to react with h^+_{vb} to oxidize –CH_2-OH to CH=O + 2 H^+, in the H_2 case, photoinduced h^+_{vb} and e^-_{cb} no longer exist in the single-electron form that can be readily observed by ESR. Rather, they either recombine or react with the same H_2 molecule. The H-H bond that can be decomposed into $[LA\text{-}H]^-$ and $[LB\text{-}H]^+$ in solid FLPs on the c-In_2O_3 surface by irradiation is thus experimentally confirmed in this work.
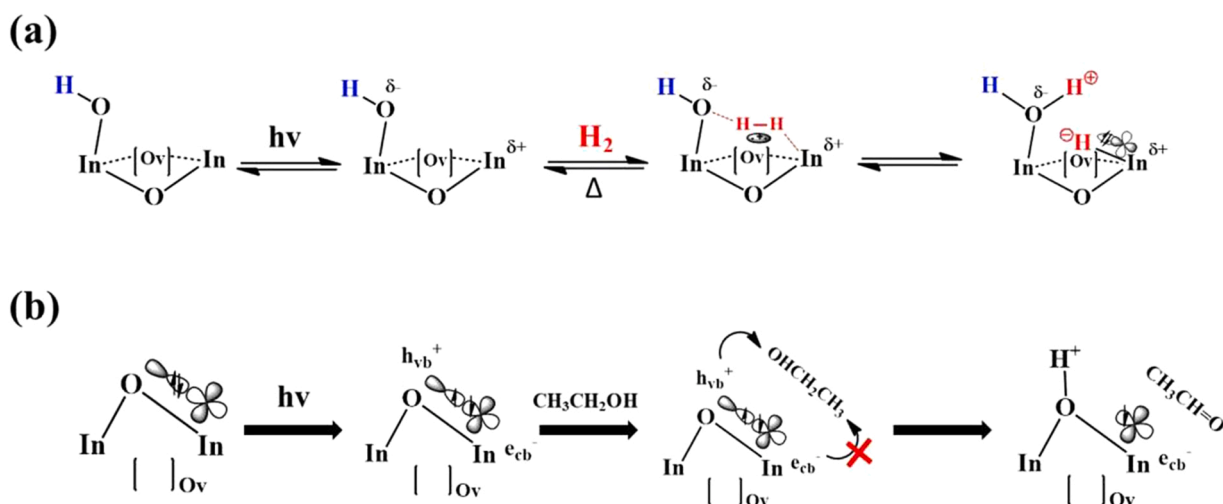
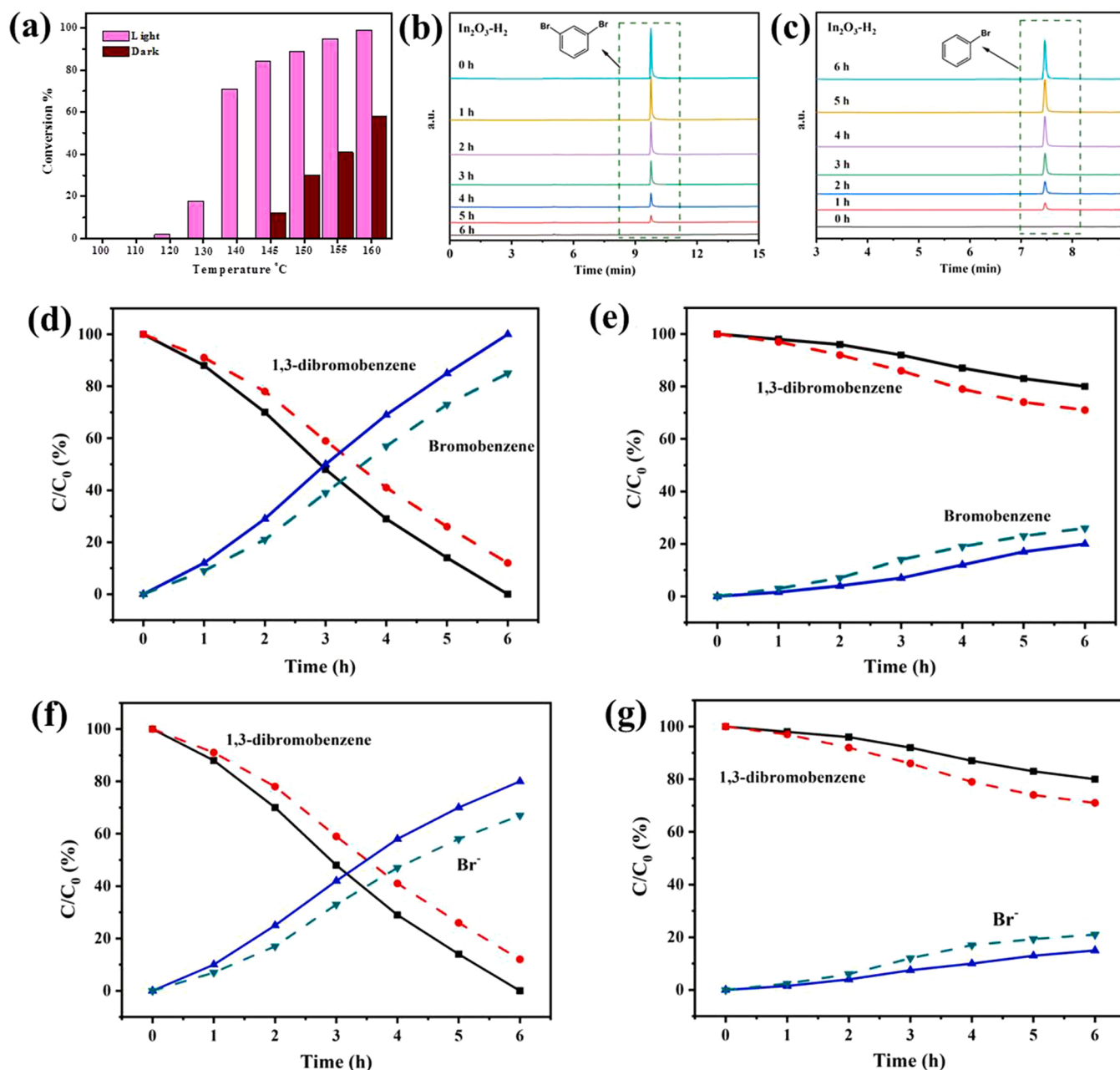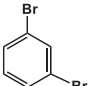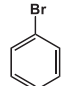**Scheme 2.** Photocatalytic dissociation pathway of H_2 (a) and ethanol (b) by c-In_2O_3.
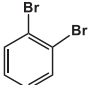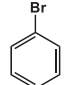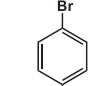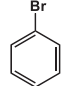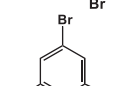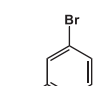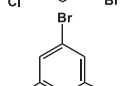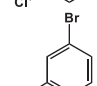
Fig. 2. Investigations of the photocatalytic dehalogenation performance of c-In$_2$O$_3$ nanoparticles. (a) The temperature-dependent behaviors of 1,3-dibromobenzene hydrogenation conversion catalyzed by the c-In$_2$O$_3$ nanoparticles for 4 h upon irradiation or in the dark. (b-c) GC-ECD spectra for the photocatalytic dehalogenation of 1,3-dibromobenzene (b) and the formation of bromobenzene (c) during the reaction at 140 °C. (Measurements of 1,3-dibromobenzene (b) and bromobenzene (c) are not shown in the same GC-ECD spectrum because of the large difference in ECD signals between the two compounds. The samples were diluted fifty times before the detection of 1,3-dibromobenzene with a split ratio of 1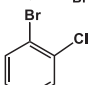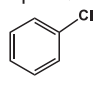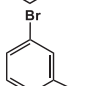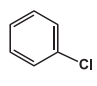:150. For the determination of bromobenzene, the samples were not diluted, and the split ratio was 1:5.) (d-g) Time-dependent evolution of the photocatalytic dehalogenation of 1,3-dibromobenzene and the formation of bromobenzene and bromide ions when irradiated in the presence of H$_2$/D$_2$ (d, f) and ethanol-d_0/ethanol-d_6 (e, g) at 140 °C. The solid lines and dashed lines indicate that the reaction was performed in H$_2$/ethanol-d_0 or D$_2$/ ethanol-d_6, respectively.

3.3. Photocatalytic dehalogenation of aryl halides by formed FLPs and H/D kinetic isotope effect studies

Given that c-In$_2$O$_3$ can definitely predecompose the H-H bond into potential [LA-H]$^-$ and [LB-H]$^+$ moieties upon irradiation in the absence of substrates, we next focus on the hydrogenation nature of such a solid-FLP. Thus, a series of hydrogenation dehalogenation reactions with H$_2$ catalyzed by c-In$_2$O$_3$ upon irradiation were investigated first. It is known that some halogenated organics, such as aryl halides, are scarcely transformed by conventional homogeneous P-B FLP catalysts [8].

Indeed, aryl halide compounds are very difficult to hydrogenate by c-In$_2$O$_3$ catalysts suspended in decane solvent without irradiation. Even when the reaction system is heated above 140 °C, the dehalogenation reaction of 1,3-dibromobenzene does not take place (see Fig. 2a). Accordingly, we selected 140 °C as a suitable reaction temperature for our photocatalytic reactions to avoid the effect of thermocatalysis. We first chose 1,3-dibromobenzene as a model compound and observed its time-dependent evolution during In$_2$O$_3$-photocatalyzed H$_2$ decomposition. As seen in Figs. 2a-b, 1,3-dibromobenzene readily reacted along with H$_2$ decomposition on c-In$_2$O$_3$ nanoparticles upon irradiation once

Table 1
Photocatalytic dehalogenation of various aromatic halides upon irradiation with H_2 or ethanol at 140 °C.

Entry	Substrate	Product	Conv. [H] (%) [a]	Conv. [E] (%) [a]	KIE [H] [b]	KIE [E] [b]
1	1,3-dibromobenzene	bromobenzene	> 99.9	21.3	1.20	0.62
2	1,2-dibromobenzene	bromobenzene	98.8	48.2	1.16	0.78
3	1,4-dibromobenzene	bromobenzene	92.0	23.3	1.30	0.85
4	1-chloro-3,5-dibromobenzene	1-bromo-3-chlorobenzene	89.1	27.4	1.19	0.86
5	1-fluoro-3,5-dibromobenzene	1-bromo-3-fluorobenzene	85.8	28.1	1.23	0.82
6	1-bromo-2-chlorobenzene	chlorobenzene	72.4	25.7	1.14	0.76
7	1-bromo-3-chlorobenzene	chlorobenzene	79.9	23.4	1.27	0.89

[a] Conv. [H] and Conv. [E] represent the average percent conversion of substrates in H_2 and ethanol, respectively. [b] KIE [H] and KIE [E] represent the KIE values of substrates in H_2 and ethanol, respectively (σ < ± 5%). Reaction conditions: c-In_2O_3 (0.2 g), decane (15 mL), substrate (2.5 mmol/L).

the reaction temperature reached 140 °C. In addition, the products of hydrogenated dehalogenation, both bromobenzene and Br^- ions, were determined by GC (Fig. 2c) and IC (Fig. S6), respectively, and were produced in proportion to the decrease in substrate (see the solid lines in Figs. 2d and 2 f). This successful hydrogenated dehalogenation of 1, 3-dibromobenzene indicated that the c-In_2O_3 photocatalyst can indeed split H_2 and insert into the C-Br bond to form C-H and HBr upon irradiation, although it is not known whether it is through [LA-H]$^-$ and [LB-H]$^+$ of solid FLPs on c-In_2O_3. More confidently, other aryl halides were used in this photocatalytic route with H_2 decomposition, and all substrates were smoothly converted as expected (Table 1), suggesting that this photocatalytic dehalogenation has certain universality.

Currently, it is very important to clarify the mechanism of this kind of hydrogenation reaction. For this purpose, we investigated the H/D kinetic isotope effect (KIE) of the hydrogenation evolution in the presence of H_2 and D_2 during c-In_2O_3 photocatalysis. As the typically homogeneous P-B FLP does not initiate these hydrogenation reactions of aryl halides, we cannot directly compare the H/D primary KIE between our solid-In_2O_3 FLP and homogeneous P-B to determine whether H^+ or H^- is transferred first. However, photocatalytic dehalogenations of these aryl halides by metal oxide semiconductors with alcohol as a hole scavenger have been well studied, as have reactions with proton transfer occurring first, in previous work by our group [60]. This reaction route exclusively results in inverse secondary H/D KIEs (i.e., KIE<1) because the change from sp^2 to sp^3-hybridization of the aryl ring is the rate-limiting step (see Fig. 3a). Encouraged by these results, we here employed ethanol-d_0/ethanol-d_6 as a hole scavenger under otherwise identical conditions to compare its KIE features with the H_2/D_2 case. Thus, a normal or inverse H/D KIE feature may suggest the order of transfer of the proton of [LB-H]$^+$ or the hydride ion of [LA-H]$^-$ to the substrates. As shown in Fig. 2, when 1,3-dibromobenzene was used as the model substrate, its hydrogenation dehalogenation with ethanol as a hole scavenger by the c-In_2O_3 photocatalyst upon irradiation occurred

successfully, similar to the H_2 case (see the solid lines in Fig. 2e and g). As expected, a typical inverse secondary KIE was observed when we used ethanol-d_6 instead of ethanol-d_0 (see the dotted lines in Fig. 2e and g); namely, the deuteration of 1,3-dibromobenzene was faster than hydrogenation (H/D KIE=0.62; see Table 1, entry 1). Regardless of the decrease in substrate or the generation of products, the inverse secondary H/D KIEs were almost uniform, indicating that after H/D incorporation into the aryl ring, the change in hybridization to lead to aromatization was the rate-limiting step (see Fig. 3a). Conversely, when we used D_2 instead of H_2, the photocatalytic hydrogenation dehalogenation with H_2 was slightly faster than that with D_2 and exhibited normal primary KIE values (H/D KIE=1.2; see Table 1, entry 1). A small primary H/D KIE close to but always greater than 1 indicates that neither the cleavage of the H-H bond nor the proton transfer first that dominates the change of sp^2- into sp^3-hybridization of the aryl ring is the rate-limiting step. Likewise, when we used the formation of dehalogenation products with H_2 and D_2, bromobenzene and bromide ions, respectively, to determine the KIE values, the same normal primary KIE values were observed (H/D KIE~1.2). Moreover, other organic halide substrates were used to further confirm the two diverse KIE features resulting from H_2/D_2 and ethanol-d_0/ethanol-d_6 (Table 1, entries 2–7). As seen in Table 1, after irradiation for 6 h, the photocatalytic dehalogenation performance of these dibrominated substrates (Table 1, entries 1–5) was superior to that of the mono-brominated substrates with one chloride (Table 1, entries 6–7). Despite remarkable differences in the absolute rates, all reactions (entries 2–7) (based on the conversion rates after irradiation for 4 h) exhibited normal H/D KIE values (within 1.1–1.3 at room temperature) in H_2/D_2, coinciding exactly with the 1, 3-dibromobenzene case (entry 1). These results undoubtedly indicated that the cleavage of H-H/D-D bonds is rarely involved in the rate-limiting step of the reaction. In contrast, although the reaction in ethanol-d_0/ethanol-d_6 displayed lower photocatalytic performance than that in H_2/D_2, all the samples exhibited distinct inverse secondary KIE
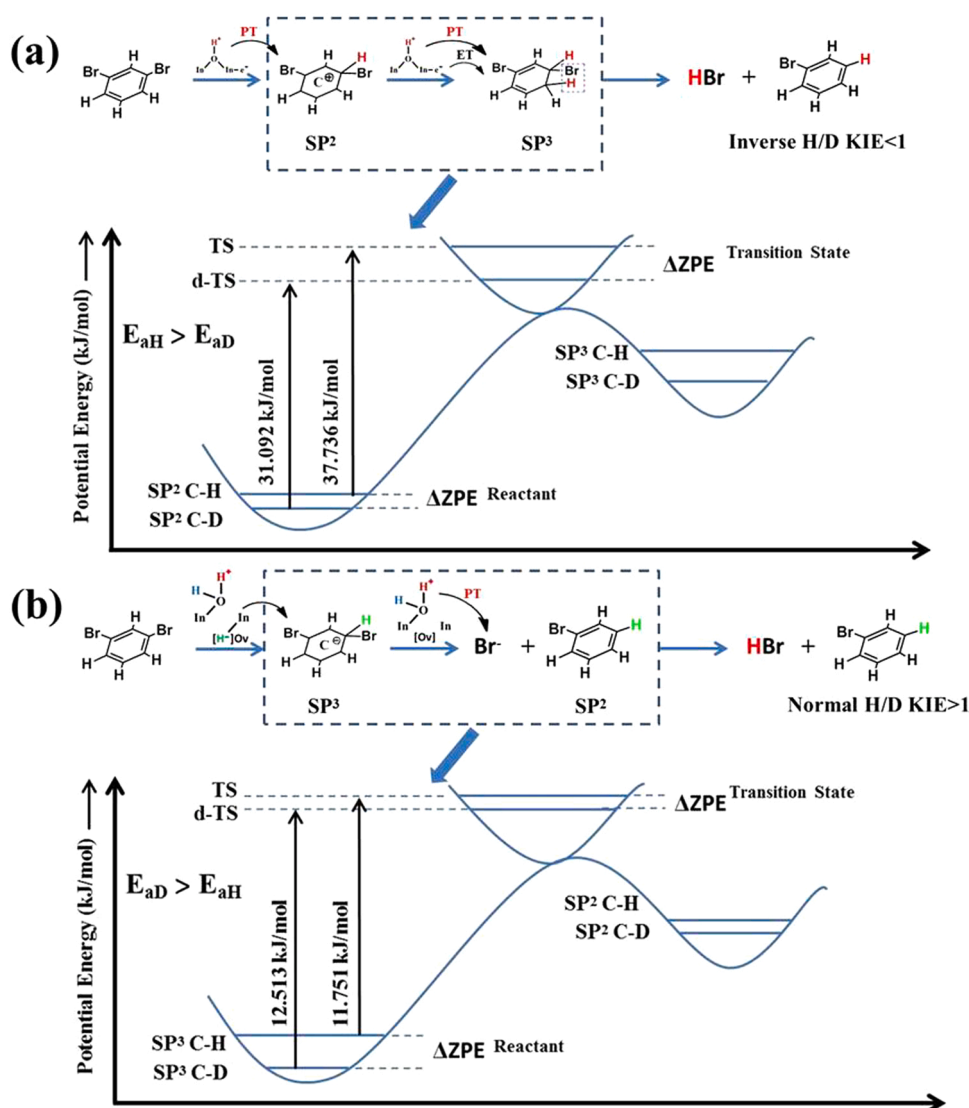
Fig. 3. Schematic diagram. Hydrogenation pathways and reaction potential energy diagrams for the photocatalytic dehalogenations of 1,3-dibromobenzene by c-In_2O_3 samples under irradiation with ethanol (a) and H_2 (b) as the hydrogen source.

values, indicating that the rate-limiting step indeed correlated with the change from sp^2- to sp^3-hybridization in the transition state (Table 1). The significant difference in the rate-limiting step between the two cases indicates that the hydrogenation mediated by c-In_2O_3 FLPs with H_2 is no longer proton transfer first dominating the change of sp^2 to sp^3 hybridization.

c-In_2O_3, as a photocatalyst in the photocatalytic hydrogenation of aryl halides with alcohol, exhibits very typical secondary inverse KIE phenomena, the mechanism of which has been well addressed by other researchers and our group [50,61–64] (see Fig. 3a). Based on the H/D KIE results, we tentatively correlate the as-formed $[LB-H]^+/[LA-H]^-$ moieties of c-In_2O_3 with H_2 splitting for the hydrogenated dehalogenation reaction of aryl halides, as shown in Fig. 3b (top), in which the substrate should be nucleophilically attacked by H^- sites first. To investigate this, we separately determined the temperature-dependent rates (Arrhenius plots) for both reactions in H_2/D_2 and ethanol-d_0/ethanol-d_6 (see Fig. S7). The difference in the activation energies (ΔEa) between the reactions in ethanol and H_2 was 25.99 kJ/mol, possibly because the hydride ion transfer occurred first, illustrating that the dehalogenation reaction with H_2 was easier. Given that homogeneous thermal FLP catalysis does not initiate this hydrogenated dehalogenation reaction of aryl compounds with H_2 splitting, we can infer that if it

could, it would be the same as the alcohol case mediated by c-In_2O_3 photocatalysis since homogeneous thermal FLP catalysis always involves H^+ transfer first. In addition, Cycling experiments for the hydrogenated dehalogenation of 1,3-dibromobenzene as well as the XRD and TEM measurements for recovered samples were performed to study the stability of as-prepared c-In_2O_3 nanoparticles in this work. As shown in Fig. S8, the conversion rate of 1,3-dibromobenzene did not exhibit evident loss after five recycles. Moreover, as shown in Fig. S9 and Fig. S10, the c-In_2O_3 samples after using did not exhibit evident changes compared to the original samples. These results undoubtedly indicate that the as-prepared c-In_2O_3 samples are effective and stable catalysts.

4. Conclusion

In summary, in this work, using MAS ^1H NMR and ESR spectroscopy, we demonstrated the distinct formation of a solid FLP structure on the c-In_2O_3 surface through heterogeneous cleavage of H-H bonds upon irradiation. More importantly, through detailed studies of a series of hydrogenated dehalogenation reactions as well as H/D kinetic isotope effects, we demonstrated that the as-formed In_2O_3 FLP-catalyzed dehalogenation reactions displayed significantly different hydrogen transfer features from the traditional alcohol in photoinduced hole scavenger

cases. Hydride ion transfer prior to proton transfer results in higher activity and greater efficiency than those of traditional FLP catalysis. Our results provide insight into the characteristics of hydride ion transfer of solid-FLPs to activate some inert substrates for hydrogenation applications.

CRediT authorship contribution statement

Zhen Wan: Investigation, Methodology, Data curation, Writing – original draft. **Chengjun Wang**: Investigation, Methodology, Data curation. **Chun Yang**: Investigation, Methodology. **Dongge Ma**: Investigation, Data curation. **Hongwei Ji**: Investigation, Conceptualization, Data curation. **Chuncheng Chen**: Investigation, Conceptualization, Supervision. **Wanhong Ma**: Investigation, Conceptualization, Methodology, Supervision, Writing – review & editing. **Jincai Zhao**: Investigation, Conceptualization, Methodology, Supervision, Review & editing.

Declaration of Competing Interest

The authors declare that they have no known competing financial interests or personal relationships that could have appeared to influence the work reported in this paper.

Data availability

Data will be made available on request.

Appendix A. Supporting information

Supplementary data associated with this article can be found in the online version at doi:10.1016/j.apcatb.2022.122237.

References

[1] X.Y. Tan, H.D. Wang, Recent advances in borenium catalysis, Chem. Soc. Rev. 51 (2022) 2583–2600.
[2] R.J. Gao, J.S. Xu, J. Wang, J.W. Lim, C. Peng, L. Pan, X.W. Zhang, H.M. Yang, J. J. Zou, Pd/Fe$_2$O$_3$ with electronic coupling single-site Pd-Fe pair sites for low-temperature semihydrogenation of alkynes, J. Am. Chem. Soc. 144 (2022) 573–581.
[3] S. Zhang, Z.Q. Huang, Y.Y. Ma, W. Gao, J. Li, F.X. Cao, L. Li, C.R. Chang, Y.Q. Qu, Solid frustrated-Lewis-pair catalysts constructed by regulations on surface defects of porous nanorods of CeO$_2$, Nat. Commun. 8 (2017) 15266.
[4] Z.L. Wu, Y.Q. Cheng, F.K. Tao, L.K. Daemen, G.S. Foo, L. Nguyen, X.Y. Zhang, A. Beste, A.J. Ramirez-Cuesta, Direct neutron spectroscopy observation of cerium hydride species on a cerium oxide catalyst, J. Am. Chem. Soc. 139 (2017) 9721–9727.
[5] H. Kobayashi, M. Yamauchi, H. Kitagawa, Y. Kubota, K. Kato, M. Takata, Atomic-level Pd-Pt alloying and largely enhanced hydrogen-storage capacity in bimetallic nanoparticles reconstructed from core/shell structure by a process of hydrogen absorption/desorption, J. Am. Chem. Soc. 132 (2010) 5576–5577.
[6] A. Bordet, W. Leitner, Metal nanoparticles immobilized on molecularly modified surfaces: versatile catalytic systems for controlled hydrogenation and hydrogenolysis, Acc. Chem. Res. 54 (2021) 2144–2157.
[7] D.W. Stephan, Diverse uses of the reaction of frustrated Lewis pair (FLP) with hydrogen, J. Am. Chem. Soc. 143 (2022) 20002–200014.
[8] T.T. Wang, M.T. Xu, A.R. Jupp, S.M. Chen, Z.W. Qu, S. Grimme, D.W. Stephan, Frustrated Lewis pair catalyzed hydrodehalogenation of benzyl-halides, Chem. Commun. 58 (2022) 1175–1178.
[9] D.W. Stephan, The broadening reach of frustrated Lewis pair chemistry, Science 354 (2016) aaf7229.
[10] J.S.J. McCahill, G.C. Welch, D.W. Stephan, Reactivity of "Frustrated Lewis Pairs": three-component reactions of phosphines, a borane, and olefins, Angew. Chem. Int. Ed. 46 (2007) 4968–4971.

[11] G.C. Welch, R.R.S. Juan, J.D. Masuda, D.W. Stephan, Reversible, metal-free hydrogen activation, Science 314 (2006) 1124–1126.
[12] P. Gao, S.G. Li, X.N. Bu, S.S. Dang, Z.Y. Liu, H. Wang, L.S. Zhong, M.H. Qiu, C. G. Yang, J. Cai, W. Wei, Y.H. Sun, Direct conversion of CO$_2$ into liquid fuels with high selectivity over a bifunctional catalyst, Nat. Chem. 10 (2017) 1019–1024.
[13] D.W. Stephan, G. Erker, Frustrated Lewis pairs: metal-free hydrogen activation and more, Angew. Chem. Int. Ed. 49 (2010) 46–76.
[14] D.W. Stephan, Frustrated Lewis pairs: from concept to catalysis, Acc. Chem. Res. 48 (2015) 306–316.
[15] L. Greb, P. Oña-Burgos, B. Schirmer, S. Grimme, D.W. Stephan, J. Paradies, Metal-free catalytic olefin hydrogenation: low-temperature H$_2$ activation by frustrated Lewis pairs, Angew. Chem. Int. Ed. 51 (2012) 10164–10168.
[16] C.K. Li, W.C. Zhao, J.H. He, Y.T. Zhang, W.Q. Zhang, Single-step expeditious synthesis of diblock copolymers with different morphologies by Lewis pair polymerization-induced self-assembly, Angew. Chem. Int. Ed. (2022), e202202448.
[17] J. Paradies, Metal-free hydrogenation of unsaturated hydrocarbons employing molecular hydrogen, Angew. Chem. Int. Ed. 53 (2014) 3552–3557.
[18] G. Eros, M. Hasan, P. Imre, A.R. Tibor, K. Péter, T. Gábor, S. Tibor, Expanding the scope of metal-free catalytic hydrogenation through frustrated Lewis pair design, Angew. Chem. Int. Ed. 49 (2010) 6559–6563.
[19] Y.W. Wang, W.Q. Chen, Z.P. Lu, Z.H. Li, H. Wang, Metal-free HB(C$_6$F$_5$)$_2$-catalyzed hydrogenation of unfunctionalized olefins and mechanism study of borane-mediated sigma-bond metathesis, Angew. Chem. Int. Ed. 52 (2013) 7496–7499.
[20] J. Jia, C.X. Qian, Y.C. Dong, Y.F. Li, H. Wang, M. Ghoussoub, K.T. Butler, A. Walsh, G.A. Ozin, Heterogeneous catalytic hydrogenation of CO$_2$ by metal oxides: defect engineering-perfecting imperfection, Chem. Soc. Rev. 46 (2017) 4631–4644.
[21] L. Wang, T.J. Yan, R. Song, W. Sun, Y.C. Dong, J.L. Guo, Z.Z. Zhang, X.X. Wang, G. A. Ozin, Room-temperature activation of H$_2$ by a surface frustrated Lewis pair, Angew. Chem. Int. Ed. 58 (2019) 7496–7499.
[22] Y.Y. Ma, S. Zhang, C.R. Chang, Z.Q. Huang, J.C. Ho, Y.Q. Qu, Semi-solid and solid frustrated Lewis pair catalysts, Chem. Soc. Rev. 47 (2018) 5541–5553.
[23] S. Zhang, Z.H. Zhang, Z.Q. Wang, Z.R. Li, W.B. Zheng, L.P. Fan, J. Zhang, Y.M. Hu, M.F. Luo, X.P. Wu, X.Q. Gong, W.X. Huang, J.Q. Lu, Metal-free ceria catalysis for selective hydrogenation of crotonaldehyde, ACS Catal. 10 (2020) 14560–14566.
[24] C.C. Jia, X.N. Kan, X. Zhang, G. Lin, W.G. Liu, Z.Y. Wang, S.Q. Zhu, D.X. Ju, J. Liu, Construction of frustrated Lewis pairs on TiO$_{2-x}$ derived from perovskite for enhanced photocatalytic CO$_2$ reduction, Chem. Eng. J. 427 (2022) 131554.
[25] L.B. Hoch, L. He, Q. Qiao, K. Liao, L.M. Reyes, Y.M. Zhu, G.A. Ozin, Effect of precursor selection on the photocatalytic performance of indium oxide nanomaterials for gas-phase CO$_2$ reduction, Chem. Mater. 12 (2016) 4160–4168.
[26] M. Ghoussoub, S. Yadav, K.K. Ghuman, G.A. Ozin, C.V. Singh, Metadynamics-biased ab initio molecular dynamics study of heterogeneous CO$_2$ reduction via surface frustrated Lewis pairs, ACS Catal. 6 (2016) 7109–7117.
[27] J.Y.Y. Loh, M. Shayegannia, N.P. Kherani, Enhancing optical phonon energies and persistent yield production of CO via substitutional doping in indium oxide, Appl. Catal. B Environ. 282 (2020), 119555.
[28] Z.Q. Ye, Y.M. Lin, L. Gong, The merger of photocatalyzed hydrogen atom transfer with transition metal catalysis for C-H functionalization of alkanes and cycloalkanes, Eur. J. Org. Chem. 2021 (2021) 5545–5556.
[29] B. Trang, Y.L. Li, X.S. Xue, M. Ateia, K.N. Houk, W.R. Dichte, Low-temperature mineralization of perfluorocarboxylic acids, Science 377 (2022) 839–845.
[30] A.K. Patra, A. Dutta, A. Bhaumik, Highly ordered mesoporous TiO$_2$-Fe$_2$O$_3$ mixed oxide synthesized by sol-gel pathway: an efficient and reusable heterogeneous catalyst for dehalogenation reaction, ACS Appl. Mater. Interfaces 4 (2012) 5022–5028.
[31] C.Y. Sun, W. Chang, W.H. Ma, C.C. Chen, J.C. Zhao, Photoreductive debromination of decabromodiphenyl ethers in the presence of carboxylates under visible light irradiation, Environ. Sci. Technol. 47 (2013) 2370–2377.
[32] Z. Ronen, A. Abeliovich, Anaerobic-aerobic process for microbial degradation of tetrabromobisphenol A, Appl. Environ. Microbiol. 66 (2000) 2372–2377.
[33] A.C. Gerecke, P.C. Hartmann, N.V. Heeb, H.P.E. Kohler, W. Giger, P. Schmid, M. Zennegg, M. Kohler, Anaerobic degradation of decabromodiphenyl ether, Environ. Sci. Technol. 39 (2005) 1078–1083.
[34] J.Z. He, K.R. Robmek, C.L. Alvarez, Microbial reductive debromination of polybrominated diphenyl ethers (PBDEs), Environ. Sci. Technol. 40 (2006) 4429–4434.
[35] Y.S. Keum, Q. Li, Reductive debromination of polybrominated diphenyl ethers by zerovelent iron, Environ. Sci. Technol. 39 (2005) 2280–2286.
[36] Y. Li, X.Q. Li, D.H. Han, W.L. Huang, C. Yang, New insights into the role of Ni loading on the surface structure and the reactivity of nZVI toward tetrabromo- and tetrachlorobisphenol A, Chem. Eng. J. 311 (2017) 173–182.
[37] S. Giri, M. Bhaumik, R. Das, V.K. Gupta, A. Maity, Dehalogenation of aromatic halides by polyaniline/zero-valent iron composite nanofiber: kinetics and mechanisms, Appl. Catal. B Environ. 202 (2017) 207–216.
[38] M. Lei, S. Guo, Z.Y. Wang, L.H. Zhu, H.Q. Tang, Ultrarapid and deep debromination of tetrabromodiphenyl ether over noble-metal-free Cu/TiO$_2$ nanocomposites under mild conditions, Environ. Sci. Technol. 52 (2018) 11743–11751.
[39] M. Lei, Z.Y. Wang, Y. Tang, H.M. Wang, L.H. Zhu, H.Q. Tang, Peculiar and full debromination of tetrabromodiphenyl ether on Pd/TiO$_2$: a competing route through hydro-debromination and coupling-debromination, Appl. Catal. B Environ. 275 (2020), 119093.
[40] Z. Wan, Q.H. Mao, Q. Chen, Proton-dependent photocatalytic dehalogenation activities caused by oxygen vacancies of In$_2$O$_3$, Chem. Eng. J. 403 (2021), 126389.

[41] H. Sakamoto, J. Imai, Y. Shiraishi, S. Tanaka, S. Ichikawa, T. Hirai, Photocatalytic dehalogenation of aromatic halides on Ta$_2$O$_5$-supported Pt-Pd bimetallic alloy nanoparticles activated by visible light, ACS Catal. 7 (2021) 5194–5201.

[42] T.J. Yan, N. Li, L.L. Wang, W.G. Ran, P.N. Duchesne, L.L. Wan, N.T. Nguyen, L. Wang, M.K. Xia, G.A. Ozin, Bismuth atom tailoring of indium oxide surface frustrated Lewis pairs boosts heterogeneous CO$_2$ photocatalytic hydrogenation, Nat. Commun. 11 (2020) 6095.

[43] J.P. Sheng, Y. He, M. Huang, C.W. Yuan, S.Y. Wang, F. Dong, Frustrated Lewis pair sites boosting CO$_2$ photoreduction on Cs$_2$CuBr$_4$ perovskite quantum dots, ACS Catal. 12 (2022) 2915–2926.

[44] J. Jia, C.X. Qian, Y.C. Dong, Y.F. Li, H. Wang, M. Ghoussoub, K.T. Butler, A. Walsh, G.A. Ozin, Heterogeneous catalytic hydrogenation of CO$_2$ by metal oxides: defect engineering-perfecting imperfection, Chem. Soc. Rev. 46 (2017) 4631–4644.

[45] K.K. Ghuman, T.E. Wood, L.B. Hoch, C.A. Mims, G.A. Ozin, C.V. Singh, Illuminating CO$_2$ reduction on frustrated Lewis pair surfaces: investigating the role of surface hydroxides and oxygen vacancies on nanocrystalline In$_2$O$_{3-x}$(OH)$_y$, Phys. Chem. Chem. Phys. 17 (2015) 14623–14635.

[46] Y. Magari, T. Kataoka, W.C. Yeh, M. Furuta, High-mobility hydrogenated polycrystalline In$_2$O$_3$ (In$_2$O$_3$:H) thin-film transistors, Nat. Commun. 13 (2022) 1078.

[47] H. Lee, Y.N. Choi, D.W. Lim, M.M. Rahman, Y.I. Kim, I.H. Cho, H.W. Kang, J. H. Seo, C. Jeon, K.B. Yoon, Formation of frustrated Lewis pairs in Pt$_x$-loaded zeolite NaY, Angew. Chem. Int. Ed. 12 (2015) 13080–13084.

[48] Q. Han, P. Gao, L.X. Liang, K.Z. Chen, A.Y. Dong, Z.M. Liu, X.W. Han, Q. Fu, G. J. Hou, Unraveling the surface hydroxyl network on In$_2$O$_3$ nanoparticles with high-field ultrafast magic angle spinning nuclear magnetic resonance spectroscopy, Anal. Chem. 93 (2021) 16769–16778.

[49] K.K. Ghuman, L.B. Hoch, P. Szymanski, J.Y.Y. Loh, N.P. Kherani, M.A. El-Sayed, G. A. Ozin, C.V. Singh, Photoexcited surface frustrated Lewis pairs for heterogeneous photocatalytic CO$_2$ reduction, J. Am. Chem. Soc. 4 (2016) 1206–1214.

[50] Y. Yan, W.D. Shi, Z. Yuan, S.G. He, D.M. Li, Q.B. Meng, H.W. Ji, C.C. Chen, W. H. Ma, J.C. Zhao, The formation of Ti-H species at interface is lethal to the efficiency of TiO$_2$ based dye-sensitized devices, J. Am. Chem. Soc. 139 (2017) 2083–2089.

[51] Y. Yan, W.D. Shi, W. Peng, Y.H. Lin, C.X. Zhang, L.L. Li, Y. Sun, H.X. Ju, J.F. Zhu, W.H. Ma, J.C. Zhao, Proton-free electron-trapping feature of titanium dioxide nanoparticles without the characteristic blue color, Commun. Chem. 2 (2019) 88.

[52] J.N. Schrauben, R. Hayoun, C.N. Valdez, M. Braten, L. Fridley, J.M. Mayer, Titanium and zinc oxide nanoparticles are proton-coupled electron transfer agents, Science 336 (2012) 1298–1301.

[53] N. Sui, P. Zhang, S. Cao, T.T. Zhou, T. Zhang, Nanosheet-assembled In$_2$O$_3$ for sensitive and selective ozone detection at low temperature, J. Alloy. Compd. 888 (2021), 161430.

[54] Z.H. Wang, C.L. Hou, Q.M. De, F.-B. Gu, D.M. Han, One-step synthesis of Co-doped In$_2$O$_3$ nanorods for high response of formaldehyde sensor at low temperature, ACS Sens. 3 (2018) 468–475.

[55] F.F. Wang, Q.J. Ding, J.R. Ding, Y.J. Bai, H.Y. Bai, W.Q. Fan, Frustrated Lewis pairs boosting photoelectrochemical nitrate reduction over ZnIn$_2$S$_4$/BiVO$_4$ heterostructure, Chem. Eng. J. 450 (2022), 138260.

[56] X.L. Pang, H.Y. Bai, H.Q. Zhao, W.Q. Fan, W.D. Shi, Efficient electrocatalytic oxidation of 5-hydroxymethylfurfural coupled with 4-nitrophenol hydrogenation in a water system, ACS Catal. 12 (2022) 1545–1557.

[57] Y.J. Bai, H.Y. Bai, Z.Y. Fang, X. Li, W.Q. Fan, W.D. Shi, Understanding the Z-scheme heterojunction of BiVO$_4$/PANI for photoelectrochemical nitrogen reduction, Chem. Commun. 57 (2021) 10568–10571.

[58] H.Q. Zhao, X.L. Pang, Y.F. Huang, Y.J. Bai, J.R. Ding, H.Y. Bai, W.Q. Fan, Electrocatalytic reduction of 4-nitrophenol over Ni-MOF/NF: understanding the self-enrichment effect of H-bonds 58 (2022) 4897–4900.

[59] L.B. Hoch, P. Szymanski, K.K. Ghuman, L. He, K. Liao, Q. Qiao, L.M. Reyes, Y. M. Zhu, M.A. El-Sayed, C.V. Singh, G.A. Ozin, Carrier dynamics and the role of surface defects: designing a photocatalyst for gas-phase CO$_2$ reduction, Proc. Natl. Acad. Sci. USA 50 (2016) 8011–8020.

[60] W. Chang, C.Y. Sun, X.B. Pang, H. Sheng, Y. Li, H.W. Ji, W.J. Song, C.C. Chen, W. H. Ma, J.C. Zhao, Inverse kinetic solvent isotope effect in TiO$_2$ photocatalytic dehalogenation of non-adsorbable aromatic halides: a proton-induced pathway, Angew. Chem. Int. Ed. 7 (2015) 2052–2056.

[61] Y.Z. Gong, C. Yang, H.W. Ji, C.C. Chen, W.H. Ma, J.C. Zhao, Aqueous oxidations started by TiO$_2$ photoinduced holes can be a rate-determining step, Chem. Asian J. 16 (2017) 2048–2051.

[62] Y.Z. Gong, C. Yang, H.W. Ji, C.C. Chen, W.H. Ma, J.C. Zhao, Mechanistic studies of TiO$_2$ photocatalysis and fenton degradation of hydrophobic aromatic pollutants in water, Chem. Asian J. 11 (2016) 3568–3574.

[63] J. Sommer, M. Hashoumy, J.C. Culmann, J. Bukala, Activation and carbonylation of methylcyclopentane in HF-SbF$_5$, New J. Chem. 21 (1997) 939–944.

[64] J. Jasik, D. Gerlich, J. Roithova, Probing isomers of the benzene dication in a low-temperature trap, J. Am. Chem. Soc. 136 (2014) 2960–2962.